Crystal Structure of $ClF_4^+SbF_6^-$, Normal Coordinate Analyses of ClF_4^+, BrF_4^+, IF_4^+, SF_4, SeF_4, and TeF_4, and Simple Method for Calculating the Effects of Fluorine Bridging on the Structure and Vibrational Spectra of Ions in a Strongly Interacting Ionic Solid

Karl O. Christe,*,[†,‡] Xiongzhi Zhang,[‡] Jeffrey A. Sheehy,[†] and Robert Bau[‡]

Contribution from the Propulsion Sciences and Advanced Concepts Division, Air Force Research Laboratory (AFRL/PRS), Edwards AFB, California 93524, and Loker Hydrocarbon Research Institute and Department of Chemistry, University of Southern California, Los Angeles, California 90089

Received September 11, 2000. Revised Manuscript Received April 12, 2001

Abstract: The crystal structure of the 1:1 adduct $ClF_5{\cdot}SbF_5$ was determined and contains discrete ClF_4^+ and SbF_6^- ions. The ClF_4^+ cation has a pseudotrigonal bipyramidal structure with two longer and more ionic axial bonds and two shorter and more covalent equatorial bonds. The third equatorial position is occupied by a sterically active free valence electron pair of chlorine. The coordination about the chlorine atom is completed by two longer fluorine contacts in the equatorial plane, resulting in the formation of infinite zigzag chains of alternating ClF_4^+ and *cis*-fluorine bridged SbF_6^- ions. Electronic structure calculations were carried out for the isoelectronic series ClF_4^+, BrF_4^+, IF_4^+ and SF_4, SeF_4, TeF_4 at the B3LYP, MP2, and CCSD(T) levels of theory and used to revise the previous vibrational assignments and force fields. The discrepancies between the vibrational spectra observed for ClF_4^+ in $ClF_4^+SbF_6^-$ and those calculated for free ClF_4^+ are largely due to the fluorine bridging that compresses the equatorial F−Cl−F bond angle and increases the barrier toward equatorial−axial fluorine exchange by the Berry mechanism. A computationally simple model, involving ClF_4^+ and two fluorine-bridged HF molecules at a fixed distance as additional equatorial ligands, was used to simulate the bridging in the infinite chain structure and greatly improved the fit between observed and calculated spectra.

Introduction

Binary halogen fluorides and their ions are ideally suited for studying molecular structures and bonding.[1−3] They cover a wide range of oxidation states from +I to +VII and coordination numbers from one to eight, including many examples of hypervalent compounds.[4] The following binary chlorine fluorides are known: ClF, ClF_3, and ClF_5;[5] they are amphoteric and, with strong Lewis acids, they can form adducts containing the Cl_2F^+,[6−8] ClF_2^+,[9−20] and ClF_4^+ [21,22] cations, respectively. Crystal structures, however, are known only for the ClF_2^+ salts.[15−20] Although these structures confirm the predominantly ionic nature of the adducts, strong interactions between the ClF_2^+ cations and the anions were observed which result in infinite chains, distort some of the ions and complicate the vibrational spectra. Chlorine pentafluoride also forms adducts with AsF_5 and SbF_5, but only the $ClF_5{\cdot}SbF_5$ complex is stable at room temperature.[21,22] On the basis of their vibrational spectra, a predominantly ionic structure was proposed[22,23] for the $ClF_5{\cdot}MF_5$ adducts with ClF_4^+ most likely possessing a pseudotrigonal bipyramidal structure of C_{2v} symmetry, similar to those found for isoelectronic SF_4[24] and the heavier halogen analogues BrF_4^+ [25] and IF_4^+.[26,27] In view of the significant cation−anion interactions found for the related ClF_2^+ salts,[15−20] it was desirable to confirm by X-ray diffraction the postulated C_{2v} structure for ClF_4^+, to obtain its exact geometry, and to determine the nature and influence of any interionic interactions. Electronic structure calculations were used to critically examine

† Air Force Research Laboratory.
‡ University of Southern California.

(1) Christe, K. O. *Proceedings from the XXIVth Int. Congr. Pure Appl. Chem.* [*Proc.*] **1974**, *4*, 115.
(2) Christe, K. O.; Wilson, W. W.; Drake, G. W.; Dixon, D. A.; Boatz, J. A.; Gnann, R. Z. *J. Am. Chem. Soc.* **1998**, *120*, 4711.
(3) Christe, K. O.; Curtis, E. C.; Dixon, D. A. *J. Am. Chem. Soc.* **1993**, *115*, 1520.
(4) Musher, J. L. *Angew. Chem., Int. Ed. Engl.* **1968**, *8*, 54.
(5) Greenwood, N. N.; Earnshaw, A. *Chemistry of the Elements*; Pergamon Press: Oxford, 1986; pp 964−978.
(6) Christe, K. O.; Sawodny, W. *Inorg. Chem.* **1969**, *8*, 212.
(7) Gillespie, R. J.; Morton, M. J. *Inorg. Chem.* **1970**, *9*, 811.
(8) Frenking, G.; Koch, W. *Inorg. Chem.* **1990**, *29*, 4513.
(9) Seel, F.; Detmer, O. *Angew. Chem.* **1958**, *70*, 163; *Z. Anorg. Allg. Chem.* **1959**, *301*, 113.
(10) Bartlett, N.; Lohmann, D. H. *J. Chem. Soc.* **1962**, 5253.
(11) Selig, H.; Shamir, J. *Inorg. Chem.* **1964**, *3*, 294.
(12) Christe, K. O.; Pavlath, A. V. *Z. Anorg. Allg. Chem.* **1965**, *335*, 210.
(13) Christe, K. O.; Sawodny, W. *Inorg. Chem.* **1967**, *6*, 313.
(14) Gillespie, R. J.; Morton, M. J. *Inorg. Chem.* **1970**, *9*, 616.
(15) Edwards, A. J.; Sills, R. J. C. *J. Chem. Soc. A* **1970**, 2697.
(16) Lynton, H.; Passmore, J. *Can. J. Chem.* **1971**, *49*, 2539.
(17) Antipin, M. Yu.; Ellern, A. M.; Sukhoverkhov, V. F.; Struchkov, Yu. T.; Buslaev, Yu. A. *Russ. J. Inorg. Chem.* **1988**, *33*, 171.
(18) Ellern, A. M.; Antipin, M. Yu.; Sharabarin, A. V.; Struchkov, Yu. T. *Russ. J. Inorg. Chem.* **1991**, *36*, 1278.
(19) Bougon, R.; Cicha, W. V.; Lance, M.; Neublat, L.; Nierlich, M.; Vigner, J. *Inorg. Chem.* **1991**, *30*, 102.
(20) Ellern, A. M.; Antipin, M. Yu.; Sharabarin, A. V.; Struchkov, Yu. T. *Russ. J. Inorg. Chem.* **1992**, *37*, 46.
(21) Christe, K. O.; Pilipovich, D. *Inorg. Chem.* **1969**, *8*, 391.
(22) Christe, K. O.; Sawodny, W. *Inorg. Chem.* **1973**, *12*, 2879.
(23) Christe, K. O.; Curtis, E. C.; Schack, C. J.; Cyvin, S. J.; Brunvoll, J.; Sawodny, W. *Spectrochem. Acta, Part A* **1976**, *36*, 1141.
(24) Tolles, W. M.; Gwinn, W. D. *J. Chem. Phys.* **1962**, *36*, 1119.
(25) Lind, M. D.; Christe, K. O. *Inorg. Chem.* **1972**, *11*, 608.
(26) Baird, H. W.; Giles, H. F. *Acta Crystallogr.* **1969**, *A25*, 115.
(27) Edwards, A. J.; Taylor, P. *J. Chem. Soc., Dalton Trans.* **1975**, 2174.

10.1021/ja003347a CCC: $20.00
Published on Web 06/09/2001

the previously reported crystal structures for BrF_4^+ [25] and IF_4^+,[26,27] and the vibrational spectra of the ClF_4^+, BrF_4^+, and IF_4^+ cations[22,28] and of the isoelectronic SF_4, SeF_4, and TeF_4 molecules. Furthermore, we outline a computationally simple method for modeling the influence of interionic fluorine bridging on the structure and vibrational spectra of the free ions.

Experimental Section

Crystal Structure Determination. A sample of $ClF_4^+SbF_6^-$ was prepared as previously described,[21,22] and single crystals were grown from solutions in anhydrous HF. Due to the moisture sensitivity of the crystals, a suitable crystal was selected and mounted with a drop of perfluoroether oil under a flow of cold dry nitrogen. The diffraction data were collected at −100 °C, using a Siemens/Nicolet/Syntex P21 diffractometer with Mo Kα radiation. The structure was solved by standard heavy-atom methods. The coordinates of the antimony and chlorine atoms were found from direct methods, and the atomic positions of the remaining fluorine atoms were revealed by subsequent difference Fourier maps.[29]

Theoretical Calculations. Theoretical calculations were carried out on IBM RS/6000 work stations using the Gaussian 98[30] and ACES II[31] program systems and the density functional B3LYP[32] and the correlated MP2[33] and single- and double-excitation coupled cluster methods,[34] including a noniterative treatment of connected triple excitations.[35]

It was desirable to perform the calculations for SF_4, ClF_4^+, SeF_4, BrF_4^+, TeF_4, and IF_4^+ by consistent methods. However, they involve atoms from the second, third, and fourth rows of the periodic table, and it was not clear whether a single type of atomic basis sets could be found that would give accurate results for all six compounds. Whereas there are many choices of high-quality basis sets for second- and third-row elements, the choices available for tellurium and iodine are far fewer and generally lower in quality. Consequently, several different basis sets were examined, most of which involved the use of effective-core potentials for the inner-shell electrons on the central atoms. The criteria used for determining the relative suitability of the basis sets for the present purposes was how well the experimentally observed vibrational spectra of SF_4 and SeF_4 were reproduced by the calculations. These molecules were chosen for the basis-set study because excellent experimental data are available for a comparison with the calculated frequencies and because there are many basis set choices for sulfur and selenium. Ultimately, it was found that the best results were obtained with the so-called DFT/DZVP all-electron basis sets,[36,37] supplemented with one *f* function taken from either the cc-pVTZ basis sets of Woon and Dunning[38] (exponents: S = 0.557, Cl = 0.706, Se = 0.462, Br = 0.552) or the polarization functions of Ahlrichs[39] (exponents: Te = 0.474, I = 0.486) on the heavy atoms, and the 6-311+G(2d) basis sets of Pople[40] on fluorine. The calculated Hessian matrices (second derivatives of the energy with respect to Cartesian coordinates) were converted to symmetry-adapted internal coordinates for subsequent normal coordinate analyses using the program systems GAMESS[41] and Bmtrx.[42]

Table 1. Crystal Data for $[ClF_4]^+[SbF_6]^-$

empirical formula	$ClF_{10}Sb$
formula weight	347.20
temperature	193(2) K
wavelength	0.71073 Å
crystal system	orthorhombic
space group	*Pbcm* (no. 57)
unit cell dimensions	a = 5.9546(12) Å; α = 90°
	b = 15.1717(19) Å; β = 90°
	c = 7.9598(17) Å; γ = 90°
volume	719.7(2) Å^3
Z	4
final R indices [$I > 2\sigma(I)$]	R1 = 0.0220, wR2 = 0.0493 (854 data)
R indices (all data)	R1 = 0.0227, wR2 = 0.0496 (880 data)

Results and Discussion

Crystal Structure of $ClF_4^+SbF_6^-$. $ClF_4^+SbF_6^-$ crystallizes in the orthorhombic space group *Pbcm* with the unit cell parameters given in Table 1. One hemisphere of data (3645 reflections) were collected at −100 °C, merged to give one unique octant of data (880 reflections), and refined to a final agreement factor of $R = 2.3\%$ for 854 reflections having $I > 2\theta(I)$. The crystal and structure refinement data, atomic coordinates and isotropic displacement parameters, and selected bond distances and angles are summarized in Tables 1−3, respectively. The structures of the ClF_4^+ and SbF_6^- ions and the

(28) Sawodny, W.; Birk, K.; Fogarasi, G.; Christe, K. O. *Z. Naturforsch.* **1980**, *35B*, 1137 and references therein.

(29) Sheldrick, G. M. Programs SHELX L86 and SHELX L93, University of Goettingen, Germany.

(30) Frisch, M. J.; Trucks, G. W.; Schlegel, H. B.; Scuseria, G. E.; Robb, M. A.; Cheeseman, J. R.; Zakrzewski, V. G.; Montgomery, J. A., Jr.; Stratmann, R. E.; Burant, J. C.; Dapprich, S.; Millam, J. M.; Daniels, R. E.; Kudin, K. N.; Strain, M. C.; Farkas, O.; Tomasi, J.; Barone, V.; Cossi, M.; Cammi, R.; Mennucci, B.; Pomelli, C.; Adamo, C.; Clifford, S.; Ochterski, J.; Petersson, G. A.; Ayala, P. Y.; Cui, Q.; Morokuma, K.; Malick, D. K.; Rabuck, A. D.; Raghavachari, K.; Foresman, J. B.; Cioslowski, J.; Ortiz, J. V.; Stefanov, B. B.; Liu, G.; Liashenko, A.; Piskorz, P.; Komaromi, I.; Gomperts, R.; Martin, R. L.; Fox, D. J.; Keith, T.; Al-Laham, M. A.; Peng, C. Y.; Nanayakkara, A.; Gonzalez, C.; Challacombe, M.; Gill, P. M. W.; Johnson, B.; Chen, W.; Wong, M. W.; Andres, J. L.; Gonzalez, C.; Head-Gordon, M.; Replogle, E. S.; Pople, J. A. *Gaussian 98*, revision A.6; Gaussian, Inc.: Pittsburgh, PA, 1998.

(31) Stanton, J. F.; Gauss, J.; Watts, J. D.; Nooijen, M.; Oliphant, N.; Perera, S. A.; Szalay, P. G.; Lauderdale, W. J.; Gwaltney, S. R.; Beck, S.; Balkova, A.; Bernholdt, D. E.; Baeck, K. K.; Rozyczko, P.; Sekino, H.; Hober, C.; Bartlett, R. J. *ACES II, Quantum Theory Project*; University of Florida: Integral packages included are VMOL (Almlof, J.; Taylor, P. R.), BPROPS (Taylor, P. R.), and ABACUS (Helgaker, T.; Jensen, H. J. Aa.; Jorgensen, P.; Olsen, J.; Taylor, P. R.)

(32) The B3LYP functional uses a three-parameter exchange functional of Becke (B3) [Becke, A. D. *J. Chem. Phys.* **1993**, *98*, 5648; Stephens, P. J.; Devlin, C. F.; Chabalowski, C. F.; Frisch, M. J. *J. Phys. Chem.* **1994**, *98*, 11623] and the Lee, Yang, and Parr (LYP) correlation gradient-corrected functional [Lee, C.; Yang, W.; Parr, R. G. *Phys. Rev. B* **1988**, *37*, 785].

(33) (a) Pople, J. A.; Binkley, J. S.; Seeger, R. *Int. Quantum Chem.* **1976**, *10*, 1. (b) Bartlett, R. J.; Silver, D. M. *Int. Quantum Chem.* **1975**, *9*, 183. (c) Dupuis, M.; Chin, S.; Marquez, A. In *Relativistic and Electron Correlation Effects in Molecules*; Malli, G., Ed.; Plenum: New York, 1994. (d) Frisch, M. J.; Head-Gordon, M.; Pople, J. A. *Chem. Phys. Lett.* **1990**, *166*, 275. (e) Bartlett, R. J.; Stanton, R. J. Applications of post-Hartree−Fock methods: A Tutorial. *Reviews of Computational Chemistry*; In Lipkowitz, K. B., Boyd, D. B., Eds.; VCH Publishers: New York, 1994; Vol. V.

(34) Purvis, G. D., III; Bartlett, R. J. *J. Chem. Phys.* **1982**, *76*, 1910.

(35) Raghavachari, K.; Trucks, G. W.; Pople, J. A.; Head-Gordon, M. *Chem. Phys. Lett.* **1989**, *157*, 479.

(36) These local-spin-density-optimized Gaussian basis sets were developed by Nathalie Godbout and Jan Andzelm and are made available courtesy of Cray Research, Inc. The general method by which they were developed is given in: Godbout, N.; Salahub, D. R.; Andzelm, J.; Wimmer, E. *Can. J. Chem.* **1992**, *70*, 560.

(37) Basis sets were obtained from the Extensible Computational Chemistry Environment Basis Set Database Version, as developed and distributed by the Molecular Science Computing Facility, Environmental and Molecular Sciences Laboratory which is part of the Pacific Northwest Laboratory, P.O. Box 999, Richland, WA 99352, U.S.A., and funded by the U.S. Department of Energy. The Pacific Northwest Laboratory is a multiprogram laboratory operated by Battelle Memorial Institue for the U.S. Department of Energy under Contract DE-AC06-76RLO 1830. Contact David Feller or Karen Schuchardt for further information.

(38) (a) Woon, D. E.; Dunning, T. H., Jr. *J. Chem. Phys.* **1993**, *98*, 1358. (b) Wilson, A. K.; Woon, D. E.; Peterson, K. A.; Dunning, T. H., Jr. *J. Chem. Phys.* **1999**, *110*, 7667.

(39) Polarization functions are unpublished supplements to the basis sets described in: Schafer, A.; Huber, C.; Ahlrichs, R. *J. Chem. Phys.* **1994**, *100*, 5829.

(40) Frisch, M. J.; Pople, J. A.; Binkley, J. S. *J. Chem. Phys.* **1984**, *80*, 3265.

(41) Schmidt, M. W.; Baldridge, K. K.; Boatz, J. A.; Elbert, S. T.; Gordon, M. S.; Jensen, J. H.; Koseki, S.; Matsunaga, N.; Nguyen, K. A.; Su, S. J.; Windus, T. L.; Dupuis, M.; Montgomery, J. A. *J. Comput. Chem.* **1993**, *14*, 1347.

(42) Komornicki, A. *Bmtrx*, Version 2.0; Polyatomics Research Institute: Redwood City, CA 1996.

Table 2. Atomic Coordinates ($\times 10^4$) and Equivalent Isotropic Displacement Parameters ($Å^2 \times 10^3$) for $[ClF_4]^+[SbF_6]^{-a}$

	x	y	z	U(eq)
Sb	904(1)	1402(1)	2500	15(1)
F(1)	−1565(4)	2191(1)	2500	25(1)
F(2)	−1047(4)	445(2)	2500	37(1)
F(3)	2845(4)	2392(1)	2500	26(1)
F(4)	902(3)	1429(1)	162(3)	34(1)
F(5)	3413(4)	669(1)	2500	33(1)
Cl	5883(1)	3440(1)	2500	16(1)
F(11)	4042(3)	4140(1)	2500	24(1)
F(12)	8045(4)	3987(1)	2500	25(1)
F(13)	5900(3)	3496(1)	472(2)	33(1)

[a] U(eq) is defined as one-third of the trace of the orthogonalized U_{ij} tensor.

Table 3. Bond Lengths [Å] and Angles [deg] for $[ClF_4]^+[SbF_6]^-$

Sb−F(2)	1.860(2)
Sb−F(4)	1.863(2)
Sb−F(5)	1.863(2)
Sb−F(3)	1.895(2)
Sb−F(1)	1.896(2)
Cl−F(11)	1.527(2)
Cl−F(12)	1.532(2)
Cl−F(13)	1.617(2)
Cl···F(1*)	2.43
Cl···F(3*)	2.41
F(2)−Sb−F(4)	90.97(5)
F(4)−Sb−F(4*)	177.47(9)
F(2)−Sb−F(5)	91.99(10)
F(4)−Sb−F(5)	90.78(5)
F(2)−Sb−F(3)	178.95(9)
F(4)−Sb−F(3)	89.02(5)
F(5)−Sb−F(3)	89.06(9)
F(2)−Sb−F(1)	90.49(11)
F(4)−Sb−F(1)	89.18(5)
F(5)−Sb−F(1)	177.53(9)
F(3)−Sb−F(1)	88.47(9)
F(11)−Cl−F(12)	103.08(12)
F(11)−Cl−F(13)	88.16(6)
F(12)−Cl−F(13)	88.06(6)
F(13)−Cl−F(13*)	173.92(13)
F(11)−Cl···F(3*)	85.4
F(12)−Cl···F(1*)	84.0
F(1*)···Cl···F(3*)	87.5

Table 4. Observed and Calculated Geometries[a] of SF_4

	obsd[b]	calcd[c]		
		B3LYP	MP2	CCSD(T)
r (S−F_{eq})	1.545(3)	1.579	1.563	1.563
r (S−F_{ax})	1.646(3)	1.681	1.660	1.657
$\langle(F_{eq}-S-F_{eq})$	101.5(5)	101.3	101.6	101.4
$\langle(F_{ax}-S-F_{ax})$	173.1(5)	172.4	171.9	171.6

[a] Bond distances in Å, angles in degrees. [b] Data from ref 24. [c] The following basis set was used for all calculations: S: DFT-DZVP; F: 6−311 + G(2d).

numbering scheme are shown in Figure 1, while the packing diagram and the interionic fluorine bridges are depicted in Figures 2 and 3, respectively.

As can be seen from Figures 1 and 2, the structure of the $ClF_5 \cdot SbF_5$ adduct is predominantly ionic consisting of discrete ClF_4^+ cations and SbF_6^- anions in a simple packing arrangement. The structure of the ClF_4^+ cation is best described as a trigonal bipyramid in which the four fluorine ligands occupy the two axial and two of the equatorial positions, while a sterically active free valence electron pair fills the third equatorial position.

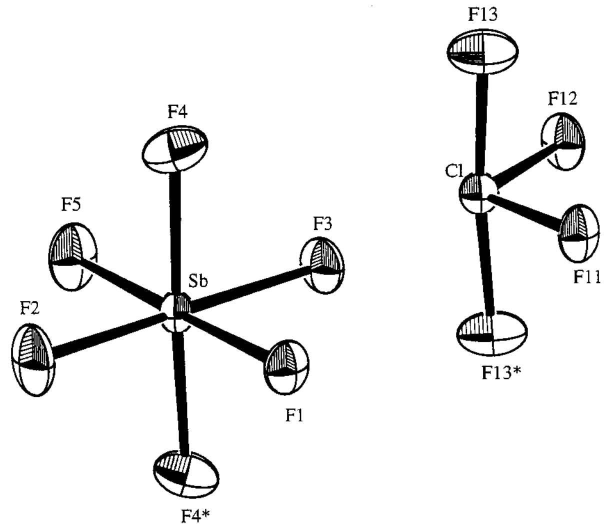

Figure 1. ORTEP plot of $ClF_4^+SbF_6^-$; thermal ellipsoids are shown at the 50% probability level.

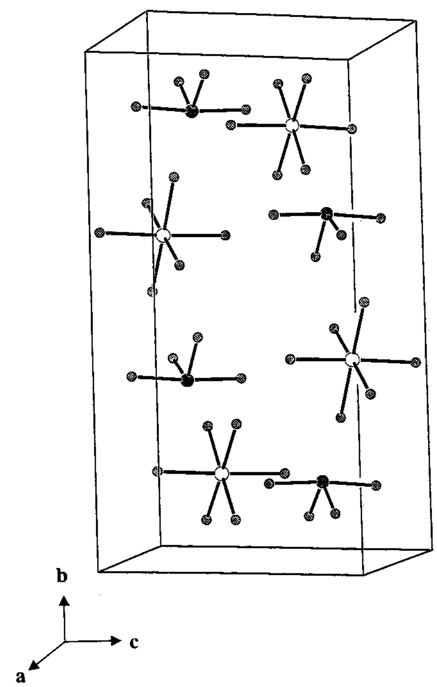

Figure 2. Packing diagram for $ClF_4^+SbF_6^-$.

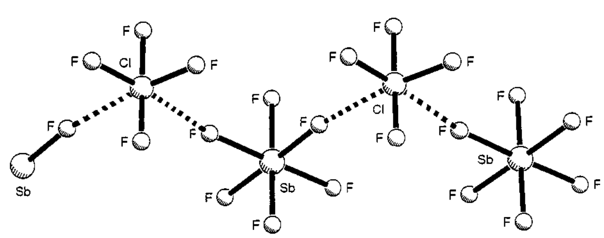

Figure 3. Interionic fluorine bridging in $ClF_4^+SbF_6^-$, showing the pseudo-octahedral fluorine environment around chlorine.

The coordination in the equatorial plane is completed by two fluorine bridges with two different SbF_6^- anions, resulting in infinite zigzag chains along the a-axis (see Figure 3). The two interionic fluorine bridges formed by each SbF_6^- anion are *cis* with respect to each other and distort the SbF_6^- octahedron from O_h to C_{2v} symmetry. The Cl−F bond lengths of the two fluorine bridges, measuring 2.41 and 2.43 Å, respectively, are comparable to those of 2.23−2.43 Å found for similar ClF_2^+ salts[15−20]

Table 5. Observed and Calculated Geometries[a] of SeF_4 and TeF_4

	SeF_4				TeF_4[c]		
	obsd[b]	calcd[d]			calcd[d]		
		B3LYP	MP2	CCSD(T)	B3LYP	MP2	CCSD(T)
r (X−F_{eq})	1.682(4)	1.718	1.701	1.703	1.879	1.862	1.866
r (X−F_{ax})	1.771(4)	1.805	1.784	1.784	1.939	1.924	1.926
$\angle$(F_{eq}−X−F_{eq})	100.6(7)	100.6	101.0	100.9	103.1	101.0	101.1
$\angle$(F_{ax}−X−F_{ax})	169.2(7)	169.2	168.1	167.5	159.4	161.2	160.5

[a] Bond distances in Å, angles in degrees. [b] Data from ref 46. [c] TeF_4 is polymeric under normal conditions (ref 60) and no experimental structure for free TeF_4 is presently known. [d] The following basis sets were used for all calculations: Se: DFT-DZVP + f(0.462); Te:DFT-DZVP + f(0.474); F: 6−311 + G(2d).

Table 6. Observed and Calculated Geometries[a] of ClF_4^+

	obsd[b]	calcd,[b] free ClF_4^+			predicted
	$ClF_4^+SbF_6^-$	B3LYP	MP2	CCSD(T)	free ClF_4^+
r (Cl−F_{eq})	1.530(2)	1.577	1.543	1.557	1.539
r (Cl−F_{ax})	1.618(2)	1.635	1.612	1.615	1.604
$\angle$(F_{eq}−Cl−F_{eq})	103.08(12)	107.8	107.1	107.7	107.7
$\angle$(F_{ax}−Cl−F_{ax})	173.92(13)	172.2	172.3	171.4	173.0

[a] Bond distances in Å, angles in degrees. [b] The following basis set was used for all calculations: Cl:DFT-DZVP + f(0.706) from cc-pVTZ; F: 6-311+ G(2d).

and are significantly shorter than the Cl−F van der Waals distance of 3.15 Å.[43] The two equatorial and the two bridging fluorines and the chlorine atoms of ClF_4^+ are perfectly planar, as shown by the sum of their bond angles of 360.0° (see Table 3).

The geometry of ClF_4^+, given in Table 3, is in accord with the VSEPR model of molecular geometry.[44] In an AX_4E-type species, such as ClF_4^+, the crowding of the axial positions results in longer and more ionic axial bonds, while the more repulsive electron pair domain[45] of the equatorial free valence electron pair E causes compressions of the equatorial F−Cl−F angle from the ideal 120° to 103° and of the axial F−Cl−F angle from 180° to 174°.

Structure Calculations for Free Gaseous ClF_4^+, BrF_4^+, IF_4^+, and Isoelectronic SF_4, SeF_4, TeF_4. Since the geometries and vibrational frequencies of SF_4[24,28] and SeF_4[46] are well-known, these molecules were used to evaluate the quality of different basis sets at the B3LYP,[32] MP2,[33] and CCSD(T)[34,35] levels of theory, with the DFT-DZVP basis[36,37] giving the best results. As can be seen from Tables 4 and 5, the MP2 and CCSD(T) calculations gave almost identical results. The density functional B3LYP method duplicated best the observed bond angles, but slightly overestimated the bond lengths.

The observed and calculated geometries of ClF_4^+ are summarized in Table 6. Scaling the calculated Cl−F bond lengths with correction factors derived from the SF_4 data of Table 4 gives for free ClF_4^+ the predicted values shown in Table 6. The major discrepancies between these values and the ones, observed for ClF_4^+ in solid $ClF_4^+SbF_6^-$ are the compression of the equatorial angle by about 4° and an increase in the difference between the axial and the equatorial bond lengths by about 2.3 pm in $ClF_4^+SbF_6^-$. These changes can be attributed to the influence of the two equatorial fluorine bridges from two neighboring SbF_6^- anions. This conclusion is supported by model calculations for the bridged ClF_4^+ cation (see below).

The minimum-energy structure of ClF_4^+ had been disputed in several previous publications. Thus, Ungemach and Schaefer predicted, on the basis of SCF calculations with minimum and double-ζ basis sets, that ClF_4^+ should be square-pyramidal.[47] In a Note Added in Proof, however, they state that the inclusion of d functions resulted in a minimum-energy structure of C_{2v} symmetry with r Cl−F_{ax} = 1.63 Å, r Cl−F_{eq} = 1.57 Å, $\angle F_{ax}$−Cl−F_{ax} = 169.6°, and $\angle F_{eq}$−Cl−F_{eq} = 109.7°. The C_{2v} structure was confirmed by So.[48] However, he surprisingly found that the axial bond (1.570 Å) was shorter than the equatorial one (1.632 Å) and his F_{eq}−Cl−Cl−F_{eq} bond angle of 117.42 ° was also very different from that given by Ungemach and Schaefer. The C_{2v} geometry given by Ungemach and Schaefer was confirmed by several subsequent studies.[49−52] It was also shown[49] that at the RHF/DZP level the energy difference between the minimum energy C_{2v} structure and the square-pyramidal C_{4v} structure, which represents the transition state for the equatorial−axial ligand exchange by the Berry mechanism, is only 6.7 kcal mol^{-1}, while a square-planar D_{4h} structure was found to lie 59.5 kcal/mol above C_{2v}.[49] Surprisingly, however, the same study[49] found that at the MP2/DZP level the D_{4h} structure becomes energetically favored over the C_{2v} structure by 16.2 kcal/mol.

In our calculations, it was found that the C_{2v} structure was the minimum energy structure at the B3LYP, MP2, and CCSD(T) levels of theory with all the basis sets used. Duplication of previous computations showed that the omission of d-functions from basis sets indeed results in a square-pyramidal C_{4v} structure being the minimum. This is not surprising in view of the small energy difference of ∼7 kcal/mol between the C_{2v} and C_{4v} structures. However, the big change of 75.7 kcal/mol reported[49] for the difference between the C_{2v} and D_{4h} structures on going from the RHF to the MP2 level could not be confirmed.

Table 7 gives a comparison between the observed and calculated structures of BrF_4^+ and IF_4^+. For IF_4^+, the deviations between the observed and calculated values agree with those noted for ClF_4^+ but are more pronounced due to increased fluorine bridging. For BrF_4^+, however, the observed bond lengths are much too long, and also the axial bond angle is too big. These large deviations, together with the extremely large uncertainties in the crystal structure of $BrF_4^+Sb_2F_{11}^-$,[25] demonstrate the need for a re-determination of its crystal structure.

Structure Calculations for Fluorine-Bridged ClF_4^+ in Solid $ClF_4^+SbF_6^-$. In many predominately ionic structures,

(43) Bondi, A. *J. Phys. Chem.* **1964**, *68*, 441.
(44) Gillespie, R. J.; Hargittai, I. *The VSEPR Model of Molecular Geometry*; Allyn and Bacon: Boston, 1991; p 55.
(45) Gillespie, R. J.; Robinson, E. A. *Angew. Chem., Int. Ed. Engl.* **1996**, *35*, 5, 495.
(46) Bowater, I. C.; Brown, R. D.; Burden, F. R. *J. Mol. Spectrosc.* **1968**, *28*, 454.
(47) Ungemach, S. R.; Schaefer, H. F., III. *J. Am. Chem. Soc.* **1976**, *98*, 1658; *Chem. Phys. Lett.* **1976**, *38*, 407.
(48) So, S.-P. *J. Chem. Soc., Faraday Trans. 2* **1981**, *77*, 213.
(49) Pershin, V. L.; Boldyrev, A. I. *J. Mol. Struct. (THEOCHEM)* **1987**, *150*, 171.
(50) Minyaev, R. M. *Russ. J. Inorg. Chem.* **1993**, *38*, 1300.
(51) Minyaev, R. M.; Wales, D. J. *J. Chem. Soc., Faraday Trans.* **1994**, *90*, 1831.
(52) Schleyer, P.v. R.; Mauksch, M. Private communication.

Table 7. Observed and Calculated Geometries[a] for BrF_4^+ and IF_4^+

	BrF_4^-				IF_4^+			
	obsd[b]	calcd[d]			obsd[c]	calcd[d]		
	$BrF_4^+Sb_2F_{11}^-$	B3LYP	MP2	CCSD(T)	$IF_4^+Sb_2F_{11}^-$	B3LYP	MP2	CCSD(T)
r (X−F$_{eq}$)	1.77(12)	1.700	1.672	1.683	1.77(3)	1.838	1.818	1.823
r (X−F$_{ax}$)	1.86(12)	1.749	1.728	1.732	1.85(4)	1.875	1.861	1.863
∠(F$_{eq}$−X−F$_{eq}$)	95.5(50)	105.9	104.9	105.4	92.4(12)	106.8	103.8	104.2
∠(F$_{ax}$−X−F$_{ax}$)	173.5(61)	168.8	168.2	167.2	160.3(12)	158.3	161.2	160.3

[a] Bond distances in Å, angles in degrees. [b] Data from ref 25. [c] Averaged bond lengths from ref 27. [d] The following basis sets were used for all calculations: Br: DFT-DZVP + f(0.552) from cc-pVTZ; I: DFT-DZVP + f(0.486); F: −311 + G(2d).

Table 8. Geometries[a] of $ClF_4^+{\cdot}2HF$ and Free ClF_4^+ Compared to That of ClF_4^+ in $ClF_4^+SbF_6$

	calculated,[b] B3LYP		observed[c]
	free ClF_4^+	$ClF_4^+{\cdot}2HF$	$ClF_4^+SbF_6^-$
(Cl−F$_{eq}$)	1.577	1.582	1.530(2)
(Cl−F$_{ax}$)	1.635	1.653	1.618(2)
(F$_{eq}$−Cl−F$_{eq}$)	107.8	100.8	103.08(12)
(F$_{ax}$−Cl−F$_{ax}$)	172.2	172.8	173.92(13)

[a] Bond distances in Å, angles in degrees. [b] The same basis set as in Table 6 was used. [c] Data from this study.

consisting of coordination-wise unsaturated cations and saturated fluoro- or oxofluoro-anions, strong fluorine bridging is observed between the anions and cations. These fluorine bridges fill empty coordination sites of the cation and, at the same time, lower the symmetry of the anions. These effects profoundly influence the vibrational spectra of these compounds. They give rise to additional bands in the anion spectra due to the symmetry lowering from O_h to C_{2v} and create new vibrations due to the bridge bonds. Although the existence of these bridges has been well established through crystal structure studies, their influence on the vibrational spectra has previously not been analyzed in sufficient detail, and as a result, the vibrational assignments of the bridging modes have in most cases either been ignored or been poor guesses. This is not surprising because the cations generally form multiple fluorine bridges with different partners, thus resulting in difficult-to-analyze infinite chains. To circumvent this problem, most previous investigators have limited their analyses to symmetry lowering of the individual ions, followed by a factor group analysis. Whereas this approach is not unreasonable for the anions, because their coordination number remains the same and their geometry does not change dramatically, it accounts neither for the structural changes in the cation nor for the newly generated bridging modes.

One possible approach to duplicate the ClF_4^+ and SbF_6^- environments in the infinite zigzag chain involves the calculation of the tri-nuclear segments (**1**) and (**2**), using the observed Cl- - -F bridge distances as the only constraints and forcing the Sb−F$_6$, Sb−F$_7$, Sb−F$_{12}$, and Sb−F$_{13}$ distances to be equal, while the remaining parameters are optimized. This approach, however, still presents the following major problems. (i) Charge neutralization and chain termination become issues. In structure **1**, the ClF_4^+ cation effectively becomes a polyanion; in structure **2**, two F^- ions, F_6^- and $F_{6'}^-$, must be added to maintain the overall negative charge and the correct coordination around the chlorine atoms but result in computationally unstable configurations that want to lose fluoride ions. (ii) Even with density functional methods and limited basis sets, the required computational effort is still large, and a vibrational analysis is complicated.

These problems were overcome in the following manner. Replacement of the two terminal SbF_6^- anions in **1** by neutral

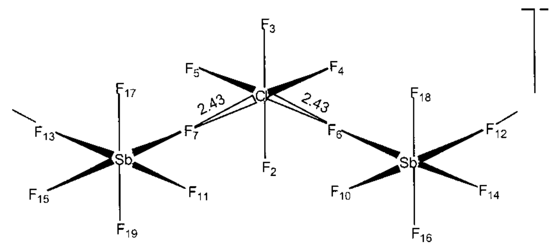

(1)

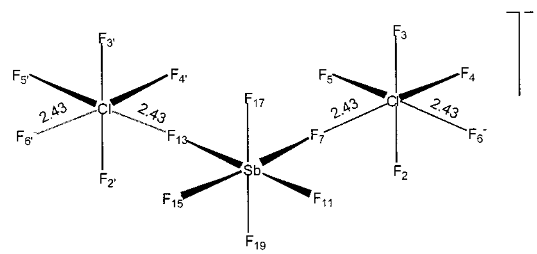

(2)

hydrogen fluoride molecules **3** maintains the positive charge of ClF_4^+ and greatly simplifies the calculation, while simulating well the two covalently bound, bridging fluorine ligands which were again constrained to the observed Cl−F bond distance of 2.43 Å.

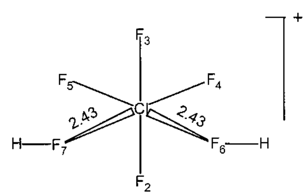

(3)

In Table 8, the geometries calculated for $ClF_4^+{\cdot}2HF$ and free ClF_4^+ at the B3LYP/B4 level are compared to that observed for ClF_4^+ in $ClF_4^+SbF_6^-$. As can be seen, the equatorial ClF_2 bond angle in $ClF_4^+{\cdot}2HF$ decreases strongly from free ClF_4^+, and the axial bond length increases, as expected for an increased ligand crowding in the equatorial plane due to the fluorine bridges. Furthermore, the bond length difference between equatorial and axial bonds increases from free ClF_4^+ to $ClF_4^+{\cdot}2HF$. All of these changes are in the same direction, as observed for ClF_4^+ in $ClF_4^+SbF_6^-$ and confirm that the discrepancies between the calculated geometry of free ClF_4^+ and the observed geometry of ClF_4^+ in solid $ClF_4^+SbF_6^-$ are mainly due to fluorine bridge bonds and not to computational shortcomings.

A comparison of the calculated geometries of $[SbF_6{-}ClF_4{-}SbF_6]^-$ and free ClF_4^+ shows that the more rigorous treatment of doubly bridged ClF_4^+ as a trinuclear segment results in similar, although more pronounced trends. Thus, on going from free ClF_4^+ to $[SbF_6{-}ClF_4{-}SbF_6]^-$, r(ClFax), r(ClFeq) and ∠(FaxClF$_{ax}$) increased by 4.5 pm, 2.7 pm, and 1.1°, respectively, while ∠(FeqClFeq) was compressed by 12.1°. It therefore

Table 9. Observed and Scaled (Unscaled) Calculated Vibrational Frequencies of SF_4

species approx mode description			frequencies, cm^{-1}			
			obsd[b]	calcd[c]		
				B3LYP	MP2	CCSD(T)
A_1	ν_1	νsym SF_2eq	892	889 (856) [117, 14p][d]	887 (904) [125, 12p]	881 (900) [120]
	ν_2	νsym SF_2ax	558	557 (537) [3.1, 12p]	558 (569) [3.2, 12p]	561 (573) [3.4]
	ν_3	sym comb of δsciss SF_2eq and ax	532	537 (494) [22, 2.1p]	539 (531) [26, 1.7p]	538 (533) [26]
	ν_4	asym comb of δsciss SF_2eq and ax	228	226 (208) [1.2, 51p]	226 (223) [1.0, 40p]	226 (224) [.89]
A_2	ν_5	τSF_2	475	473 (435) [0, 1.2dp]	471 (464) [0, 1.0dp]	470 (465) [0]
B_1	ν_6	νas SF_2ax	730	741 (714) [659, 1.1bp]	739 (753) [693, 1.2dp]	740 (756) [680]
	ν_7	δrock SF_2eq	[~532][e]	540 (497) [.21, .54dp]	539 (531) [.43, .53dp]	538 (533) [.85]
B_2	ν_8	νas SF_2eq	867	858 (827) [187, 5.0dp]	862 (879) [196, 4.3dp]	862 (881) [184]
	ν_9	δsciss SF_2ax out of plane	353	354 (326) [12, 0.1dp]	353 (348) [13, .0.6dp]	356 (352) [14]
sum of (ν obsd $\pm$ ν calcd)				34	32	45
empirical scaling factors:	ν			1.03798	0.98080	.97866
	δ			1.08696	1.01559	1.01008

[a] Separate empirical scaling factors were used for the stretching and deformation vibrations to maximize the fit between observed and calculated frequencies. [b] Data from ref 28. [c] Using basis set from Table 4. [d] Calculated infrared and Raman intensities in km/mol and Å^4/amu. [e] This band coincides with and is obscured by ν_3.

Table 10. Observed and Scaled (Unscaled) Calculated[a] Vibrational Frequencies of ClF_4^+

vibration		frequencies, cm^{-1}			
		obsd for $ClF_4^+SbF_6^-$	calcd for free ClF_4^+		
			B3LYP	MP2	CCSD(T)
A_1	ν_1	802 [vs, 10][b]	778 (769([49, 19p][c]	803 (856) [64, 11p]	774 (794) [49]
	ν_2	574 [w, 6]	583 (576) [6.0.18p]	568 (605) [5.7, 13p]	583 (598) [4.7]
	ν_3	515 [sh, 0.2]	506 (475) [21, 3.1p]	515 (526) [26, 1.7p]	508 (509) [24]
	ν_4	235 [−, 0.5]	150 (141) [.55, 1.1wp]	166 (169) [.69, .76wp]	159 (159) [.50]
A_2	ν_5	475 [−, 1]	488 (458) [0, 2.4dp]	488 (498) [0, 2.0dp]	488 (489) [0]
B_1	ν_6	803 [vs, ?]	841 (831) [437, .11dp]	809 (862) [478, .23dp]	833 (855) [428]
	ν_7	534 (505), [5.5, 1.2dp]	538 (505) [5.5, 1.2dp]	541 (552) [7.3, 1.0dp]	537 (538) [8.7]
B_2	ν_8	822 [s, 2.5]	798 (788) [116, 5.0dp]	824 (878) [146, 2.9dp]	810 (831) [102]
	ν_9	386 [m, −]	379 (356) [15, .23dp]	371 (379) [18, .14dp]	379 (380) [18]
sum of (ν obsd $\pm$ ν calcd)			213	119	185
empirical scaling factors:[d]	ν		1.0122	.9836	0.97457
	δ		1.06576	.97969	0.99788

[a] Using basis set from Table 6. [b] Observed relative infrared and Raman intensities. [c] Calculated infrared and Raman intensities in km/mol and Å^4/amu. [d] ν_4 was omitted from the calculation of the scaling factors for the deformation modes.

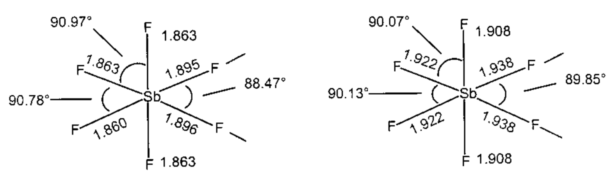

Figure 4. Observed (a) and calculated (b) structures of C_{2v} distorted SbF_6^-.

appears that the simplified model with HF bridging groups approximates the binding in ClF_4SbF_6 better than the more elaborate tri-nuclear model.

Modeling the SbF_6^- distortion was simpler. The only constraint imposed on SbF_6^- was forcing the two equatorial Sb−F bonds that are involved in the *cis*-fluorine bridging to be 3 pm longer than the two axial Sb−F bonds (the same amount as that observed in the crystal structure) and allowing the rest of the structure to maximize. The resulting structure is compared in Figure 4 to that observed for the crystal structure of ClF_4-SbF_6. The calculated structure exhibits angle changes, similar to but less pronounced than those observed for SbF_6^- in ClF_4-SbF_6. This can be attributed to the fact that in the calculated structure the Sb−F bonds *trans* to the fluorine bridges also become somewhat longer (*trans*-effect), and therefore, the angle deviations from 90° become smaller.

Vibrational Spectra. SF_4. The observed and unscaled and scaled calculated vibrational spectra of SF_4 are listed in Table 9. The scaled B3LYP, MP2, and CCSD(T) frequencies fit about equally well, but the MP2 and CCSD(T) sets require less scaling.

The assignment of the vibrational spectra of SF_4 on the basis of experimental data alone had been a most difficult and frustrating task and required at least 13 publications from several different laboratories.[28] Despite all of this previous work, our present study reveals that even in the most recent reassignment[28] there are still two errors. The infrared inactive Raman band observed at 475 cm^{-1} must be $\nu_5(A_2)$, and the infrared inactive $\nu_7(B_1)$ Raman band should occur at about 540 cm^{-1} and is apparently hidden by the two very intense Raman bands, $\nu_2(A_1)$ and $\nu_3(A_1)$ at 558 and 532 cm^{-1}, respectively. This reassignment results in an excellent fit between observed and calculated spectra, particularly if it is kept in mind that no anharmonicity corrections have been applied to the observed frequencies.

ClF_4^+. Table 10 compares the vibrational frequencies calculated for free gaseous ClF_4^+ to those observed for solid $ClF_4^+SbF_6^-$. As expected, the agreement is not as good as for isoelectronic SF_4 where gas phase values were compared. However, the agreement is still very satisfactory and shows that the previously proposed[22] assignments are correct. As for SF_4, the MP2 set gives the best frequency fit, and the CCSD(T) set requires the least scaling. The agreement between the observed

Table 11. Scaled (Unscaled) Vibrational Frequencies of Free Gaseous ClF_4^+ and $ClF_4^+{\cdot}2HF$, Calculated at the B3LYP Level, Compared to Those Observed for $ClF_4^+SbF_6^-$

mode		approx mode description	obsd in $ClF_4^+SbF_6^-$	calculated	
				free ClF_4^+	$ClF_4^+{\cdot}2HF$[b]
A_1	ν_1	νsym ClF_2eq	802	778 (769)	794 (766) [147, 50p]
	ν_2	νsym ClF_2ax	574	583 (576)	577 (557) [7.9, 20p]
	ν_3	δsciss ClF_2eq and ax, sym combination	515	506 (475)	517 (476) [60, 2.3p]
	ν_4	δsciss ClF_2eq and ax, antisym combination	235	150 (141)	225 (206)[c] [.96, .92p]
A_2	ν_5	τClF_2	475	488 (458)	470 (439) [0, 1.9dp]
B_1	ν_6	νas ClF_2ax	803	841 (831)	831 (802) [481, .47dp]
	ν_7	δrock ClF_2eq	534	538 (505)	538 (496) [1.9, .89dp]
B_2	ν_8	νas ClF_2eq	822	798 (788)	798 (770) [167, 15dp]
	ν_9	δsciss ClF_2ax out of plane	386	379 (356)	399 (367) [39, .08dp]
$\Sigma\Delta$ (ν obsd $\pm$ ν calcd)				213	92
scaling factors:	ν			1.01222	1.036575
	δ			1.06576	1.08544

[a] Empirical scaling factors to maximize the fit. [b] The two Cl−F contacts between ClF_4^+ and 2HF were constrained to 2.42 Å, the observed Cl−F bridge distance in $ClF_4^+SbF_6^-$. [c] This mode couples with the symmetric ClF_2 bridge stretching mode as a symmetric and an antisymmetric combination of the corresponding symmetry coordinates. The listed frequency of 206 cm^{-1} is the average of the calculated values of 185 and 227 cm^{-1} (see Table 12).

and the calculated MP2 values is better than 16 cm^{-1} for all modes, except for $\nu_4(A_1)$ where the discrepancy of 69 cm^{-1} is huge. This mode represents the anti-symmetric combination of the axial and the equatorial scissoring motions (**4**) and is

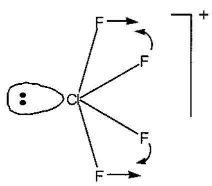

(4)

responsible for the inversion of the axial and the equatorial ligands by the Berry pseudorotation mechanism.[54] As was pointed out already above and is also transparent from structure **1**, the two equatorial fluorine bridges impede these motions and thereby increase the frequency of this mode and raise the barrier to the equatorial−axial ligand exchange in the solid.

The influence of the fluorine bridges in solid $ClF_4^+SbF_6^-$ on the vibrational frequencies of ClF_4^+ was modeled, as described above for the geometries, at the B3LYP level with two bridging HF ligands. The results are summarized in Table 11 and show that the large discrepancy of 85 cm^{-1} between the calculated frequency of ν_4 for free ClF_4^+ and the observed one in $ClF_4^+SbF_6^-$ is indeed due to the fluorine bridging. For the bridged $ClF_4^+{\cdot}2HF$ model, the discrepancy between the calculated and the observed frequencies of ν_4 shrinks to 13 cm^{-1}, and the fit of the remaining eight frequencies was also greatly improved by 46 cm^{-1}. This result demonstrates that typical fluorine bridges, as encountered in many main group fluoride salts, cannot be ignored in a thorough analysis, and that our simple model of using HF to replace large counterions and infinite chains is well suited for simulating the observed frequencies.

As pointed out above, most previous analysis had failed to correctly identify and assign the fluorine-bridging modes in the infinite-chain, fluorine-bridged salts. Table 12 summarizes the results from our normal coordinate analysis of $ClF_4^+{\cdot}2HF$. As a nine-atomic species, it has 21 normal modes. Of these, six are associated with hydrogen motions (see footnote a) of Table 12) and are of little interest for our analysis, because hydrogen has been used only as a simulator for an SbF_5 group and the

Table 12. Calculated Unscaled Fluorine Bridge Modes in $ClF_4^+{\cdot}2HF$[a]

		approximate mode description in symmetry C_{2v}	B3LYP freq [IR, Ra int]
A_1	ν_1'	antisymmetric and symmetric combinations of the symmetric ClF_{2BR} stretch and the ClF_4^+ Berry mode ν_4	227 [0.96, .92p] 185 [1.0, 2.5p]
	ν_2'	δsciss ClF_{2BR}	62 [3.2, .48p]
A_2	ν_3'	δpucker 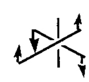	55 [0, 1.2dp]
B_1	ν_4'	δrock ClF_{2BR}	71 [49, 1.6dp]
B_2	ν_5'	νas ClF_{2BR}	178 [11, .97dp]
	ν_6'	δas ClF_{2BR} in plane	132 [0.2, .02dp]

[a] In addition to these six modes, the following six modes were identified which involve hydrogen displacements: 3951, νH−F, in-phase; 3947, νH−F, out-of-phase; 308, δwag H, in-phase; 301, δwag H, out-of-phase; −83, δrock H, out-of-phase; −38, δrock H, in-phase.

Sb−F modes are already included in the analysis of the (C_{2v}) SbF_6^- ion. It should be noted that the two rocking modes involving the hydrogen atoms have imaginary frequencies because constraining the Cl−F bridge bond length to the observed value resulted in a maximized geometry that is not a global minimum. The remaining 15 modes can be separated into nine fundamentals for ClF_4^+ (see Table 11) and six fundamentals for the fluorine bridges (see Table 12). The six fundamentals for the fluorine bridge modes are highly characteristic, except for the symmetric ClF_{2BR} mode, $\nu_1'(A_1)$, which strongly couples with the Berry mode, $\nu_4(A_1)$, of ClF_4^+ (see footnote c of Table 11), due to their similar motions and frequencies. These mixings of the S3 and S4 symmetry coordinates of ClF_4^+ and of S4 of ClF_4^+ with S1′ of fluorine-bridged ClF_4^+ account for most of the difficulties encountered with attempts to fit the observed vibrational spectra with less

(53) Christe, K. O.; Sawodny, W.; Pulay, P. *J. Mol. Struct.* **1974**, *21*, 158.

(54) Berry, R. S. *J. Chem. Phys.* **1960**, *32*, 933.

Table 13. Observed and Scaled[a] (Unscaled) Calculated Vibrational Frequencies (cm^{-1}) of SeF_4 and TeF_4

		SeF_4				TeF_4			
		obsd	calcd			obsd	calcd		
vibration[b]			B3LYP	MP2	CCSD(T)		B3LYP	MP2	CCSD(T)
A_1	ν_1	744	743(723)[60,16p][c]	740(761)[63,15p]	736(754)[59]	695	680(674)[56,16p]	681(704)[59]	680(102)[57]
	ν_2	574	581(565)[1.7,14p]	579(596)[0.94,14p]	580(595)[0.75]	572	572(567)[0.02,12p]	570(590)[0]	570(589)[0.07]
	ν_3	367	369(339)[25,1.2p]	370(366)[30,1.1p]	372(369)[31]	293	294(271)[33,0.96p]	297(291)[39]	297(291)[40]
	ν_4	162	169(155)[1.6,0.58wp]	168(166)[1.4,0.50p]	167(165)[1.4]	–	107(99)[1.1,0.38wp]	125(122)[0.9]	125(122)[0.9]
A_2	ν_5	374	372(342)[0,1.6dp]	373(369)[0,1.4dp]	372(367)[0]	–	323(298)[0,1.3dp]	313(307)[0]	312(305)[0]
B_1	ν_6	634	635(618)[378,0.73dp]	636(654)[392,0.92dp]	637(653)[381]	588	606(600)[257,1.8dp]	607(628)[275]	607(627)[268]
	ν_7	409	407(374)[10,1.0dp]	407(402)[15,0.95dp]	400(405)[16]	333	332(306)[15,0.84dp]	329(322)[19]	328(321)[20]
B_2	ν_8	733	724(705)[117,5.6dp]	729(750)122,5.0dp]	730(748)[114]	682	676(670)[104,5.9dp]	677(700)[104]	678(700)[101]
	ν_9	256	248(228)[14,0.02dp]	247(244)[14,0.02dp]	249(246)[15]	–	222(205)[14,0]	199(195)[15]	199(195)[15]
$\Sigma\Delta(\nu$ obsd $\pm$ ν calcd)			39	36	43		41	48	49
empirical scaling	ν		1.02765	0.97188	0.97557		1.00947	0.9668	0.96831
factors	δ		1.08754	1.01176	1.01176		1.08471	1.02055	1.02213

[a] Empirical scaling factors. [b] The approximate mode description is identical to that given in Table 9. [c] Infrared and Raman intensities in km/mol and $Å^4$/AMU, respectively.

Table 14. Observed and Scaled[a] (Unscaled) Calculated Vibrational Frequencies (cm^{-1}) of BrF_4^+ and IF_4^+

		BrF_4^+				IF_4^+		
		obsd	calcd			calcd		
vibration[b]			B3LYP	MP2	CCSD(T)	B3LYP	MP2	CCSD(T)
A_1	ν_1	723	718(721)[23,21p]	729(783)[31,13p]	708(738)[21]	(716)[25,20p]	(757)[30,17p]	(740[24]
	ν_2	606	622(625)[2,18p]	612(658)[1.5,14p]	623(650)[0.94]	(650)[0.02,16p]	(673)[0.0007,16p]	(667)[0.005]
	ν_3	369	366(351)[21,1.5p]	368(385)[25,1.1p]	368(377)[25]	(295)[28,1.1p]	(311)[32,0.97p]	(313)[33]
	ν_4		137(131)[0.71,0.97wp]	141(147)[0.7,8p]	139(143)[0.62]	(97)[0.6,0.58wp]	(119)[0.56, 0.52p]	(134)[0.61]
A_2	ν_5	385	388(372)[0,2.5dp]	386(403)[0,2.3dp]	386(396)[0]	(332)[0,2.1dp]	(339)[0,1.9dp]	(336)[0]
B_1	ν_6	736	730(733)[253,0.16dp]	716(769)[272,0.3dp]	731(762)[242]	(709)[179,1.1dp]	(734)[202,0.9dp]	(732)[186]
	ν_7		414(397)[12,1.4dp]	411(430)[16,1.3dp]	410(420)[16]	(333)[15,1.1dp]	(351)[19,1.2dp]	(353)[19]
B_2	ν_8	736	729(732)[68,5.6dp]	743(798)[86,3.4dp]	737(768)[59]	(734)[68,5.7dp]	(773)[71,4.9dp]	(758)[57]
	ν_9		272(261)[13,0.06dp]	262(274)[14,0.04dp]	269(276)[14]	(237)[13,0.0007dp]	(220)[14,0.009dp]	(215)[14]
$\Sigma\Delta(\nu$ obsd $\pm$ ν calcd)			40	41	40			
empirical scaling	ν		.99548	0.93128	0.95905			
factors	δ		1.04311	0.95689	0.97550			

[a] Empirical scaling factors. [b] The approximate mode description is identical to that given in Table 9.

rigorous analyses. Inspection of Tables 11 and 12 demonstrates that the bridging modes in $ClF_4^+SbF_6^-$ occur below 230 cm^{-1} and, therefore, interfere only with the lowest-frequency mode of ClF_4^+. Since most of the bridging modes of solid $ClF_4^+SbF_6^-$ occur in the range of the lattice modes, reliable observation and analysis of these modes are presently not possible.

SeF_4. Table 13 shows a comparison of the observed and calculated vibrational frequencies of free gaseous SeF_4. The listed observed frequencies are the gas-phase values,[55,56] except for that of ν_9 which was observed only as a very weak and broad band.[55] For this mode the averaged frequency of the molecule isolated in different matrices[55] was used. As in the case of gaseous SeF_4 (Table 9), the agreement between observed and calculated frequencies is excellent, and for the MP2 set, the scaling factors are also close to unity. These results lend strong support to our revised assignments given in Table 13. Of the previous assignments, only those given by Alexander and Beattie for six of the modes[56] are correct. In the paper by Ramaswamy,[57] seven of the nine fundamentals were assigned incorrectly; in the study by Adams and Downs,[55] six fundamentals were assigned correctly, two were assigned incorrectly, and one was missing; and in the most recent study by Seppelt of SeF_4 in CH_3F solution,[58] only four of the nine fundamentals were assigned correctly, and the latter assignments unfortunately have found their way into recent compilations, such as the book by Nakamoto.[59]

TeF_4. The observed and calculated vibrational frequencies of TeF_4 are compared in Table 13. Since TeF_4 is polymeric at room temperature,[60] the frequencies of matrix-isolated TeF_4[55] were used as the experimental values. The agreement between observed and calculated frequencies and infrared intensities is again very good, and the scaling factors are similar to those used for SeF_4. Our results confirm the experimental frequencies but show that the previous assignments[55] for $\nu_3(A_1)$ and $\nu_7(B_1)$ must be reversed.

BrF_4^+ and IF_4^+. The calculated vibrational frequencies for free gaseous BrF_4^+ and IF_4^+ are summarized in Table 14. Only partial experimental values are given for BrF_4^+, and no values are given for IF_4^+ because the reported spectra for these two cations are incomplete, their crystal structures are poorly determined, and fluorine bridging is expected to become more pronounced with increasing atomic weights of the halogen central atoms. Clearly, both cations should be thoroughly reinvestigated.

C_{2v} Distorted SbF_6^-. To judge the influence of fluorine bridging on the vibrational spectra of SbF_6^-, the spectra of octahedral SbF_6^- and of C_{2v} distorted SbF_6^- were calculated at the B3LYP level. For (O_h) SbF_6^-, r was found to be 1.923 Å, and for (C_{2v}) SbF_6^- the geometry given in Figure 4b was used.

(55) Adams, C. J.; Downs, A. J. *Spectrochim. Acta* **1972**, *28A*, 1841.
(56) Alexander, L. E.; Beattie, I. R. *J. Chem. Soc., Dalton Trans.* **1972**, 1745.
(57) Ramaswamy, K.; Jayaraman, S. *Ind. J. Pure Appl. Phys.* **1970**, *8*, 625.
(58) Seppelt, K. *Z. Anorg. Allg. Chem.* **1975**, *416*, 12.
(59) Nakamoto, K. *Infrared and Raman Spectra of Inorganic and Coordination Compounds*, 5th ed.; John Wiley & Sons: New York, 1997.
(60) Edwards, A. J.; Hewaidy, F. I. *J. Chem. Soc. A* **1968**, 3977.

Table 15. Correlation Diagram for SbF_6^- ($O_h \rightarrow C_{2v}$) and Unscaled Frequencies, Infrared and Raman Intensities, and Polarization of Raman Bands Calculated at the B3LYP Level

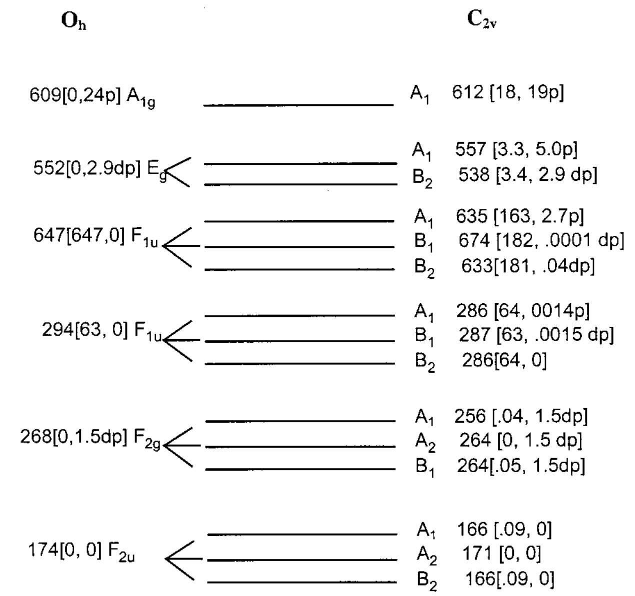

Table 16. Scaled CCSD(T) Force Constants and Potential Energy Distribution of SF_4

	calcd freq,[a] cm^{-1}			symmetry force constants[b]				potential energy[c] distribution (%)
				F_{11}	F_{22}	F_{33}	F_{44}	
A_1	ν_1	881	F_{11}	5.40				60(1), 4(2), 15(3), 21(4)
	ν_2	561	F_{22}	.78	3.81			90(2), 10(1)
	ν_3	538	F_{33}	.19	−0.01	1.22		55(4), 41(3), 3(1)
	ν_4	226	F_{44}	.45	−0.10	.60	1.49	59(3), 41(4)
A_2	ν_5	470	F_{55}	1.97				100(5)
B_1	ν_6	740	F_{66}	F_{66}	F_{77}			74(6), 26(7)
				2.99				
	ν_7	538	F_{77}	0.74	2.19			96(7), 4(6)
B_2	ν_8	862	F_{88}	F_{88}	F_{99}			89(8), 11(9)
				5.01				
	ν_9	356	F_{99}	.56	1.98			100(9)

[a] Frequencies from Table 9. [b] Stretching force constants in mdyn/Å, deformation constants in mdyn Å/rad^2, and stretch−bend interaction constants in mdyn/rad. Scaling factors: stretching force constants, $(0.97866)^2$; deformation constants, $(1.01008)^2$; stretch−bend interactions, 0.97866×1.01008. [c] The following symmetry coordinates were used: S1 = νsym eq; S2 = νsym ax; S3 = δsym eq; S4 = δsym ax; S5 = τ; S6 = νas ax; S7 = δ rock eq; S8 = νas eq; S9 = δsciss ax out-of-plane.

The calculated vibrational spectra are summarized in Table 15 and show that even relatively small distortions of about 0.15 ° for some of the angles and of about 0.03 Å for some of the bonds cause significant changes in the vibrational spectra and, particularly, in the stretching modes. A detailed analysis of the SbF_6^- part in the previously reported[22] spectra of $ClF_4^+SbF_6^-$ was not carried out due to complications caused by the presence of some $Sb_2F_{11}^-$ bands and an overlap with at least three fundamentals of ClF_4^+, although the observed spectra[22] appear to support the above conclusions.

Normal Coordinate Analyses. Normal coordinate analyses were carried out for the two isoelectronic series SF_4, SeF_4, TeF_4 and ClF_4^+, BrF_4^+, IF_4^+. The results are summarized in Tables 16−21 and show that the A_2, B_1, and B_2 vibrations are highly characteristic for all six compounds. For the A_1 block, however, strong mixing of the symmetry coordinates is observed. As previously discussed for ClF_4^+,[23] SF_4,[23,53] and PF_4^-,[61] the ν_3 and ν_4 deformation modes are symmetric and anti-symmetric combinations of the S3 and S4 symmetry coordinates, respectively. The ν_3 mode is the umbrella deformation, and ν_4 is the equatorial−axial ligand-exchange motion involved in the Berry pseudorotation mechanism.[54] In addition to this mixing of the

Table 17. Scaled CCSD(T) Force Constants and Potential Energy Distribution of SeF_4

	calcd freq,[a] cm^{-1}			symmetry force constants[b]				potential energy[c] distribution (%)
				F_{11}	F_{22}	F_{33}	F_{44}	
A_1	ν_1	736	F_{11}	4.89				84(1), 7(2), 4(3), 5(4)
	ν_2	580	F_{22}	0.39	3.89			91(2), 9(1)
	ν_3	372	F_{33}	.02	−0.02	.95		52(4), 47(3), 1(2)
	ν_4	167	F_{44}	.22	−0.22	.49	1.01	52(3), 48(4)
A_2	ν_5	372	F_{55}	1.46				100(5)
B_1	ν_6	637	F_{66}	F_{66}	F_{77}			94(6), 6(7)
				3.17				
	ν_7	400	F_{77}	0.36	1.63			100(7), 4(6)
B_2	ν_8	730	F_{88}	F_{88}	F_{99}			98(8), 2(9)
				4.69				
	ν_9	249	F_{99}	.25	1.39			100(9)

[a] Frequencies from Table 13. [b,c] Force constant dimensions and symmetry coordinates are identical to those given in the footnotes of Table 16. Scaling factors − stretching force constants, $(0.97557)^2$; deformation constants, $(1.01281)^2$: stretch−bend interaction, 0.97557×1.01281.

Table 18. Scaled CCSD(T) Force Constants and Potential Energy Distribution of TeF_4

	calcd freq,[a] cm^{-1}			symmetry force constants[b]				potential energy[c] distribution (%)
				F_{11}	F_{22}	F_{33}	F_{44}	
A_1	ν_1	680	F_{11}	4.52				90(1), 7(2), 2(3), 2(4)
	ν_2	570	F_{22}	0.23	3.69			93(2), 7(1)
	ν_3	297	F_{33}	−0.076	−0.039	.76		53(4), 47(3)
	ν_4	125	F_{44}	.17	−0.19	.48	.84	52(3), 46(4)
A_2	ν_5	312	F_{55}	1.22				100(5)
				F_{66}	F_{77}			
B_1	ν_6	607	F_{66}	3.25				98(6), 2(7)
	ν_7	328	F_{77}	0.20	1.37			100(7)
				F_{88}	F_{99}			
B_2	ν_8	678	F_{88}	4.40				99(8), 1(9)
	ν_9	199	F_{99}	.15	1.12			100(9)

[a] Frequencies from Table 13. [b,c] Force constant dimensions and symmetry coordinates are identical to those given in the footnotes of Table 16. Scaling factors − stretching force constants, $(0.96831)^2$; deformation constants, $(1.02213)^2$: stretch−bend interaction, 0.96831×1.02213.

Table 19. Scaled CCSD(T) Force Constants and Potential Energy Distribution of ClF_4^+

	calcd freq,[a] cm^{-1}			symmetry force constants[b]				potential energy[c] distribution (%)
				F_{11}	F_{22}	F_{33}	F_{44}	
A_1	ν_1	774	F_{11}	4.46				58(1), 5(2), 16(3), 21(4)
	ν_2	583	F_{22}	.47	3.97			87(2), 11(1), 1(3), 1(4)
	ν_3	508	F_{33}	.020	−0.027	.73		62(4), 34(3), 4(1)
	ν_4	159	F_{44}	.46	−0.018	.60	1.35	69(3), 30(4)
A_2	ν_5	488	F_{55}	2.01				100(5)
				F_{66}	F_{77}			
B_1	ν_6	833	F_{66}	3.89				77(6), 23(7)
	ν_7	537	F_{77}	0.69	2.21			98(7), 2(6)
				F_{88}	F_{99}			
B_2	ν_8	810	F_{88}	4.53				89(8), 11(9)
	ν_9	379	F_{99}	.69	2.03			100(9)

[a] Frequencies from Table 10. [b,c] Force constant dimensions and symmetry coordinates are identical to those given in the footnotes of Table 16. Scaling factors − stretching force constants, $(0.97457)^2$; deformation constants, $(0.99788)^2$: stretch−bend interaction, 0.97457×0.99788.

(61) Christe, K. O.; Dixon, D. A.; Mercier, H. P. A.; Sanders, J. P. C.; Schrobilgen, G. J.; Wilson, W. W. *J. Am. Chem. Soc.* **1994**, *116*, 2850.

Table 20. Scaled CCSD(T) Force Constants and Potential Energy Distribution of BrF_4^+

	calcd freq,[a] cm^{-1}		symmetry force constants[b]				potential energy[c] distribution (%)
			F_{11}	F_{22}	F_{33}	F_{44}	
A_1 ν_1	708	F_{11}	4.68				84(1), 7(2), 4(3), 5(4)
ν_2	623	F_{22}	.15	4.40			91(2), 9(1)
ν_3	368	F_{33}	−0.009	.012	.70		60(4), 40(3)
ν_4	139	F_{44}	.27	−0.11	.49	.98	62(3), 38(4)
A_2 ν_5	386	F_{55}	1.48				100(5)
			F_{66}	F_{77}			
B_1 ν_6	731	F_{66}	4.12				93(6), 7(7)
ν_7	410	F_{77}	.35	1.65			100(7)
			F_{88}	F_{99}			
B_2 ν_8	737	F_{88}	4.74				97(8), 3(9)
ν_9	269	F_{99}	.36	1.44			100(8)

[a] Frequencies from Table 14. [b,c] Force constant dimensions and symmetry coordinates are identical to those given in the footnotes of Table 16. Scaling factors − stretching force constants, $(0.95905)^2$; deformation constants, $(0.97550)^2$: stretch−bend interaction, 0.95905 × 0.97550.

Table 21. Scaled CCSD(T) Force Constants and Potential Energy Distribution of IF_4^+

	calcd freq,[a] cm^{-1}		symmetry force constants[b]				potential energy[c] distribution (%)
			F_{11}	F_{22}	F_{33}	F_{44}	
A_1 ν_1	710	F_{11}	5.01				92(1), 5(2), 1(3), 2(4)
ν_2	640	F_{22}	.056	4.59			95(2), 5(1)
ν_3	307	F_{33}	.011	.046	.73		57(4), 43(3)
ν_4	131	F_{44}	.23	−0.088	.46	.87	43(4), 57(3)
A_2 ν_5	329	F_{55}	1.30				100(5)
			F_{66}	F_{77}			
B_1 ν_6	703	F_{66}	4.32				98(6), 2(7)
ν_7	345	F_{77}	.23	1.37			100(7)
			F_{88}	F_{99}			
B_2 ν_8	728	F_{88}	5.07				99(8), 1(9)
ν_9	211	F_{99}	.24	1.19			100(9)

[a] Empirical scaling factors of 0.96 and 0.98 were used for the stretching and deformation modes, respectively. [b,c] Force constant dimensions and symmetry coordinates are identical to those given in the footnotes of Table 16. Scaling factors − stretching force constants, $(0.96)^2$; deformation constants, $(0.98)^2$: stretch−bend interaction, 0.96 × 0.98.

Table 22. Stretching Force Constants (mdyn/Å) of ClF_4^+ and SF_4 Compared to Those of PF_4^-, SeF_4, TeF_4, BrF_4^+, and IF_4^+

	PF_4^-	SF_4	SeF_4	TeF_4	ClF_4^+	BrF_4^+	IF_4^+
fr, eq	3.94	5.21	4.79	4.46	4.50	4.77	5.04
frr	.26	.20	.10	.06	−0.035	−0.03	−0.03
fR, ax	1.82	3.40	3.53	3.47	3.93	4.26	4.46
fRR	.34	.41	.36	.22	.04	.14	.14
fR + fr	5.76	8.61	8.32	7.93	8.43	9.03	9.50
fR/fr	.46	.65	.74	.78	.87	.89	.88

deformation modes, ν_1 which is mainly equatorial stretching, contains strong contributions from S3 and S4 that decrease with increasing mass of the central atom.

The force constants of greatest interest are the internal equatorial and axial stretching force constants (see Table 22 and Figure 5). The data show that the force constants of the axial bonds (*fR*) are significantly smaller than those of the equatorial bonds (*fr*). This fact is in accord with the corresponding bond lengths and can be explained by strong contributions from semi-ionic, 3center-4electron bonding[63−65] to the axial bonds. The extent of semi-ionic bonding in the XF_4 molecules

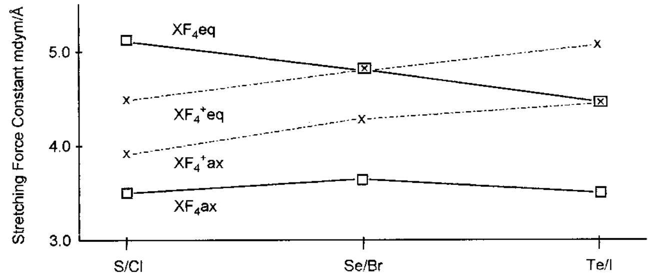

Figure 5. Stretching-force constants of the axial and equatorial bonds in the isoelectronic SF_4, SeF_4, TeF_4 (solid lines) and ClF_4^+, BrF_4^+, IF_4^+ (broken lines) series.

can be judged from *fR*/*fr*, the ratio of the axial force constant divided by the equatorial force constant, and ideally should approach 0.5, as shown for PF_4^- (*fR*/*fr* = 0.46).

For the ClF_4^+, BrF_4^+, IF_4^+ series, the overall bond strength, (*fR* + *fr*), increases from ClF_4^+ to IF_4^+, and the ratio of semi-ionic to covalent bonding, (*fR*/*fr*), is practically constant. Therefore, the slopes of the two XF_4^+ curves in Figure 5 are positive and very similar. For the SF_4, SeF_4, TeF_4 series, the overall bond strength is opposite. They decrease from SF_4 to TeF_4, while the contribution from semi-ionic bonding increases from TeF_4 to SF_4, thus accounting for the negative slope of *fr* and the larger differences between *fr* and *fR*. On going from ClF_4^+ to PF_4^- the contribution from semi-ionic 3c-4e bonding strongly increases. This can be attributed mainly to the increasing formal negative charge that favors the formation of semi-ionic bonds. The increasing contribution of semi-ionic bonding from TeF_4 to SF_4 can be explained by the different axial F-X-F bond angles. Semi-ionic bonds are ideally linear as they involve only one *p*-orbital of the central atom, and the axial bond angle increases significantly from TeF_4 to SF_4 (see Tables 4 and 5). There must be an opposite effect, however, that is most pronounced for the XF_4^+ cations, as the contribution from semi-ionic bonding remains almost constant in spite of changes in the axial bond angles similar to those in the neutral XF_4 series. This difference is attributed to the increased effective electronegativity of the central atom that is most pronounced for the XF_4^+ cations. Among these isoelectronic terafluorides, the central atoms in the XF_4^+ cations possess the highest electronegativities and the highest oxidation state of (+V), and a decreasing difference in the effective electronegativities between the central atom and the ligands favors covalent over semi-ionic bonding. These results demonstrate that care must be exercised when comparing trends within an isoelectronic series.

Another important point must be made concerning the force fields. In all of the previously published force fields, the value of F_{44}, the axial, in-plane bending force constant, had been badly underestimated by about 50% due to the undetermined nature of the previous A_1 block force constant solutions and the tempting low frequencies of ν_4. The high values, found for F_{44} in this study, are in much better agreement with the well-determined[62] value of F_{99}, the axial out-of-plane bending force constant. On the basis of Gillespie's model of points of equal repulsion on a sphere,[43] the values of F_{44} and F_{99} should be of similar magnitude.

Conclusions

This paper provides the first comprehensive and conclusive study of the $ClF_5 \cdot SbF_5$ adduct. It shows that $ClF_5 \cdot SbF_5$ is ionic, containing discrete ClF_4^+ and SbF_6^- ions that are interconnected and distorted by fluorine bridges. The ClF_4^+ cation has a

(62) Christe, K. O.; Willner, H.; Sawodny, W. *Spectrochim. Acta* **1979**, *35A*, 1347.
(63) Pimentel, G. C. *J. Chem. Phys.* **1951**, *19*, 446.
(64) Hach, R. J.; Rundle, R. E. *J. Am. Chem. Soc.* **1951**, *73*, 4321.
(65) Rundle, R. E. *J. Am. Chem. Soc.* **1963**, *85*, 112.

pseudotrigonal bypyramidal structure, in accord with the VSEPR predictions[43,44] and the known structure of isoelectronic SF_4.[24] The results of this study are supported by electronic structure calculations for the ClF_4^+, BrF_4^+, IF_4^+ and the isoelectronic SF_4, SeF_4, TeF_4 series. They permit a reassignment of the observed vibrational spectra and an analysis of their trends. Our results also show that the previously reported experimental structures and vibrational analyses of BrF_4^+ and IF_4^+ are inaccurate or incomplete and need to be repeated. Furthermore, it is shown that in these compounds fluorine bridging strongly distorts the individual ions. A simple method for modeling this bridging is described and can account for most of the differences between the experimental geometry and vibrational spectra of $ClF_4^+SbF_6^-$ and those predicted for the free isolated ions.

Acknowledgment. We thank the National Science Foundation and the Air Force Office of Scientific Research for financial support.

Supporting Information Available: Tables of structure determination summary, atomic coordinates, bond lengths and angles and anisotropic displacement parameters of ClF_4SbF_6 in CIF format. This material is available free of charge via the Internet at http://pubs.acs.org.

JA003347A